energies

MDPI

Article

A Data-Driven Control Parameter Optimization Framework for Enhancing Frequency Stability in High-Renewable-Penetration Power Systems

Lin Cheng [1], Fengrui Yang [1,*], Zhou Xing [2], Jing Ren [2], Zhe Zhang [1] and Gengfeng Li [1]

[1] School of Electrical Engineering, Xi'an Jiaotong University, Xi'an 710049, China; zz1248@stu.xjtu.edu.cn (Z.Z.); gengfengli@xjtu.edu.cn (G.L.)
[2] Northwest Branch of State Grid Corporation of China, Xi'an 710048, China
* Correspondence: yangfr@stu.xjtu.edu.cn; Tel.: +86-153-3905-0010

Abstract

As the penetration rate of renewable energy continues to rise, the equivalent inertia of power systems has significantly decreased, leading to a marked degradation in frequency stability support capabilities. Under conditions of high renewable energy penetration, the question of how to effectively enhance grid frequency support capacity has become a critical research topic in the field of power system operation and control. This paper first systematically analyzes the impact of key control parameters on the frequency dynamic response of power systems. It investigates the intrinsic relationship between these parameters and system frequency stability through both analytical frequency response modeling and time-domain simulation analysis. A frequency stability margin metric is constructed based on the grid frequency response process to quantify the system's frequency stability performance. Building upon this foundation, an improved ResNet-based frequency stability margin prediction model is established to enable rapid estimation of the frequency stability margin. Furthermore, Bayesian optimization is introduced to optimize frequency control parameters, thereby enhancing system frequency stability. Case studies conducted on the simulation system CSEE-FS with insufficient frequency support capability demonstrate that the proposed method effectively increases the frequency stability margin and significantly improves the system's frequency response performance.

Keywords: frequency stability margin; Bayesian optimization; droop coefficient; virtual inertia coefficient; control parameter optimization

Check for updates

Academic Editor: Guillermo Escrivá-Escrivá

Received: 30 January 2026
Revised: 23 March 2026
Accepted: 24 March 2026
Published: 1 April 2026

Copyright: © 2026 by the authors. Licensee MDPI, Basel, Switzerland. This article is an open access article distributed under the terms and conditions of the Creative Commons Attribution (CC BY) license.

1. Introduction

Amid the global transition toward green and low-carbon energy systems, the large-scale development and utilization of renewable energy has become an inevitable pathway for addressing escalating environmental pressures and energy security challenges, while simultaneously driving the coordinated advancement of related energy production sectors, such as flexible natural gas generation, as well as energy storage technologies [1,2]. China has emerged as a global leader in renewable energy deployment, particularly in wind and solar power generation. According to the latest National Electric Power Industry Statistical Data released by the National Energy Administration in 2025, China's installed wind and solar capacity reached approximately 1.4 billion kilowatts by the end of 2024, accounting for about 41.8% of the total installed power generation capacity. As a result, the integration

of high proportions of renewable energy is expected to become a defining characteristic of China's future power system [3].

While the rapid expansion of renewable energy has significantly alleviated energy scarcity and environmental concerns [4,5], it has also introduced substantial challenges to the secure and stable operation of power systems and posed new requirements for overall power system resilience [6–8]. On the one hand, the increasing penetration of inverter-based renewable energy sources has fundamentally altered system dynamics, leading to higher levels of power electronic interfacing and AC/DC hybrid interconnections [9]. Consequently, grid structures, operational modes, and existing energy system frameworks are being continuously reshaped, resulting in profound changes in transient behavior and stability mechanisms [10–12]. On the other hand, the displacement of conventional synchronous generators with high mechanical inertia has markedly reduced the system's inherent disturbance resistance. The resulting decline in frequency regulation capability has increased the vulnerability of the power system to large disturbances, thereby elevating the risk of frequency instability under high-renewable-penetration conditions.

To enhance the frequency stability support capability of power systems under high renewable energy penetration, researchers have conducted extensive studies from various perspectives. From the control strategy standpoint, scholars have proposed the concept of virtual inertia control (VIC). By simulating the swing equation of synchronous machines using grid-connected inverters, it responds to frequency variations in the form of virtual inertia, thereby improving transient frequency response [13,14]. References [15,16] employs DC-side capacitors to simulate synchronous machine inertia and primary frequency regulation characteristics, enabling converter stations to provide inertia support to AC systems. However, this method features fixed control modes with limited scalability, hindering multi-station coordination. Reference [17] proposes a variable inertia control strategy by adjusting DC voltage to enhance DC capacitor energy, thereby increasing system inertia. However, limited capacitor energy capacity risks DC voltage instability during a rapid large energy discharge. Reference [18] analyzes the inertial response characteristics of wind turbines under different control modes and investigates the impact of virtual inertia provided by wind turbines on system frequency, confirming that VSGs reduce maximum frequency change rates and improve minimum frequency points. However, most existing studies on VSG frequency support capabilities neglect the impact of actual operating states and anticipated fault scenarios of renewable energy equipment on control parameters. They typically set inertia or virtual inertia time constants as fixed values, failing to fully leverage VSG flexibility.

Given that frequency support effectiveness is highly dependent on key parameters, control parameter optimization has garnered increasing attention. References [19,20] optimized the time constant of the lowpass filter in DFIG inertia control based on trajectory sensitivity, improving the system's power angle stability and frequency stability. However, it did not account for the inertia control coefficient. References [21,22] analyzes the influence mechanism of primary frequency regulation droop coefficients and virtual inertia time constants on small disturbance stability in renewable energy systems. Reference [23] examines the primary frequency regulation characteristics of wind turbines and proposes a tuning strategy for wind power static droop coefficients. Reference [24] investigates system frequency response under uncertainty and proposes a frequency parameter tuning method for wind power that accounts for frequency stability. However, the frequency control parameter optimization methods mentioned in the above studies rarely impose direct constraints on system inertia or frequency indicators in their mathematical models. This prevents power plants from fully utilizing their inertia and frequency support capabilities after faults, failing to ensure sufficient system frequency regulation capacity to handle large-scale faults.

In summary, building upon existing studies, this paper jointly considers transient and steady-state frequency stability margin metrics and proposes a data-driven control parameter optimization method for enhancing system frequency stability based on the frequency stability margin [25,26]. First, the impacts of key control parameters on the system frequency dynamic response are investigated based on a system frequency response model [8]. Then, a frequency stability margin index is formulated, and an improved ResNet-based predictor is developed to rapidly estimate the stability margin under different operating conditions. On this basis, Bayesian optimization is employed to efficiently search for the optimal control parameter set, thereby improving the overall frequency stability performance of the power system. Finally, the effectiveness of the proposed method is validated through simulations on the simulation system CSEE-FS with insufficient frequency support capability.

2. Impact of Control Parameters on Power System Frequency Stability

2.1. Power System Frequency Dynamic Model

Figure 1 shows a general block diagram of a virtual synchronous generator (VSG) system, which comprehensively accounts for the effects of multiple control loops on the system's dynamic characteristics, including the DC-link voltage control (DVC), phase-locked loop (PLL), inner voltage and current control loops, and the virtual impedance loop. Specifically, the active power control (APC) and reactive power control (RPC) loops regulate the active and reactive power outputs to generate the corresponding phase angle and voltage magnitude references, respectively. Subsequently, the voltage loop is employed to regulate the inverter output voltage, while the current loop is primarily implemented for overcurrent limitation and active damping enhancement.

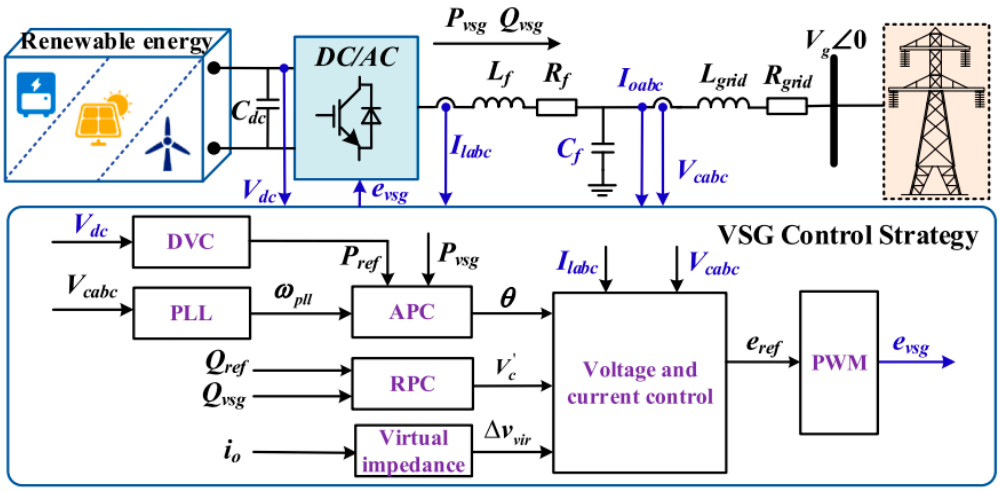


Figure 1. General system diagram of a VSG.

A small-signal model is established at the power equilibrium point at the rated frequency. This second-order system frequency response (SFR) model is based on the assumptions of small-disturbance linearization, regional frequency consistency, constant parameters, and low-order dynamics dominance. It further assumes that the governor dynamics satisfy the static droop relationship, thereby simplifying the system into a low-order dynamic model with frequency and mechanical power as state variables. The second-order SFR model and its corresponding state-space formulation can be expressed as:

$$2H\frac{d\Delta f}{dt} = \Delta P_t - \Delta P_L - D\Delta f \quad (1)$$

$$T_t \frac{d\Delta P_m}{dt} = -\Delta P_m - \frac{1}{R}\Delta f \tag{2}$$

$$\dot{x} = \begin{bmatrix} -\frac{D}{2H} & \frac{1}{2H} \\ -\frac{1}{RT_t} & -\frac{1}{T_t} \end{bmatrix} x + \begin{bmatrix} -\frac{1}{2H} \\ 0 \end{bmatrix} u \tag{3}$$

$$\begin{cases} x = \begin{bmatrix} \Delta f \\ \Delta P_m \end{bmatrix} \\ u = \Delta P_L \end{cases} \tag{4}$$

In the formula, H and D, respectively, represent the system inertia and damping coefficients; ΔP_t, ΔP_L and ΔP_m are, respectively, changes in turbine output power, load disturbances, and mechanical power increments. T_t is the time constant of the steam turbine. This second-order SFR model is suitable for analyzing region-averaged frequency dynamics dominated by inertia and primary frequency regulation over short time scales under conditions of small disturbances near the rated operating point; its accuracy is limited in scenarios involving large disturbances, rapid transients, high-order nonlinearities, and significant governor dynamics.

Based on the above equations, it can be concluded that system frequency stability is closely related to the key control parameters, such as the virtual inertia coefficient and the droop coefficient. In general, increasing the virtual inertia coefficient and the droop coefficient can enhance system frequency stability by strengthening inertial support and primary frequency regulation, respectively. Therefore, this research selects the inertia coefficient, droop coefficient, and their corresponding upper limits of power output as the optimization parameters. In this paper, the droop coefficient is set within [10, 50], the virtual inertia coefficient is set within [10, 30], and the upper limit amplitudes of both the virtual inertia control power output and the droop control power output are set within [0%, 15%]. These ranges are chosen to cover typical regulation strengths, from weak to strong support, while ensuring that the additional frequency support remains within the device's available active power capability and stable operating boundaries. Considering that excessively large virtual inertia gains may induce oscillations or even instability, moderate ranges are adopted for the droop and virtual inertia coefficients, while the ranges of the virtual inertia control power output upper limit amplitude and the droop control power output upper limit amplitude are both set to [0%, 15%], which helps ensure the physical realizability of the control output and avoids saturation or excessive dynamic impacts.

2.2. Impact of Control Parameters on Frequency Stability

Based on the power system frequency dynamic model developed in the previous section, the impacts of key control parameters, including the virtual inertia coefficient and the droop coefficient, on frequency stability can be analytically characterized. However, the derived relationships are established under simplified modeling assumptions and may be affected by practical control constraints and nonlinear dynamics. Therefore, to further validate the theoretical analysis and to qualitatively assess the influence of parameter variations on the frequency response, a simulation-based parametric sensitivity study is conducted in this section by systematically adjusting the virtual inertia coefficient, droop coefficient, and their corresponding power limit constraints.

This paper employs the low-frequency case study (The Chinese Society for Electrical Engineering-frequency stability, CSEE-FS) released by the China Electric Power Research Institute to validate the simulation system. The system structure, as shown in Figure 2, comprises 3 DC lines, 47 critical nodes, 31 AC transmission lines, and 62 transformers. The system incorporates seven conventional generating units with a total installed capacity of 5400 MW. The combined installed capacity of wind and solar power—the two primary

renewable energy sources—reaches 6900 MW, comprising 3150 MW of wind power and 3750 MW of solar power. Renewable energy accounts for 56.1% of the total installed capacity. The impacts of control parameter variations on the system stability level are analyzed, and the corresponding results are presented in Figures 3–6.

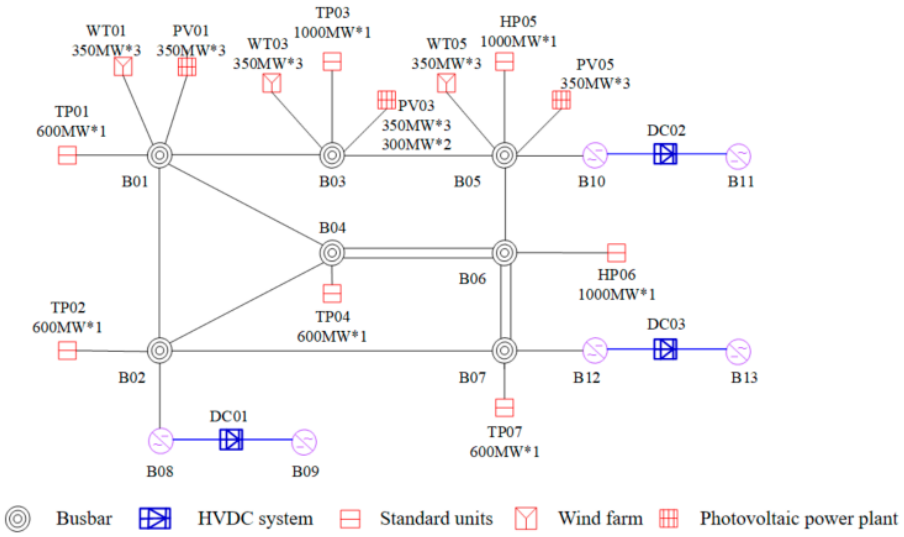


Figure 2. Low-Frequency Case Study System Architecture.

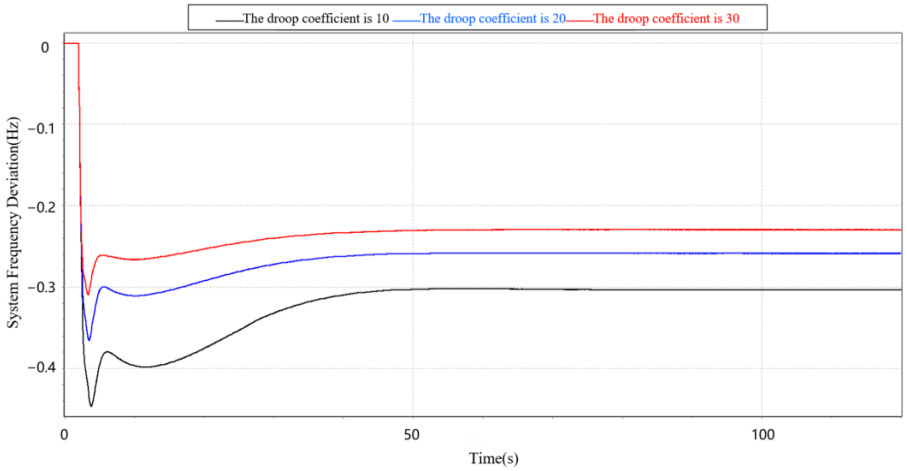


Figure 3. The influence of the droop coefficient on frequency stability.

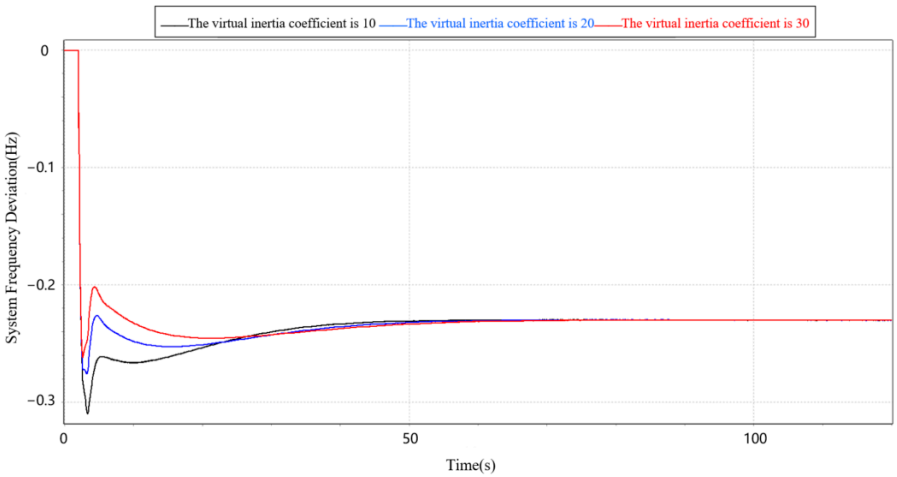


Figure 4. The influence of virtual inertia coefficient on frequency stability.

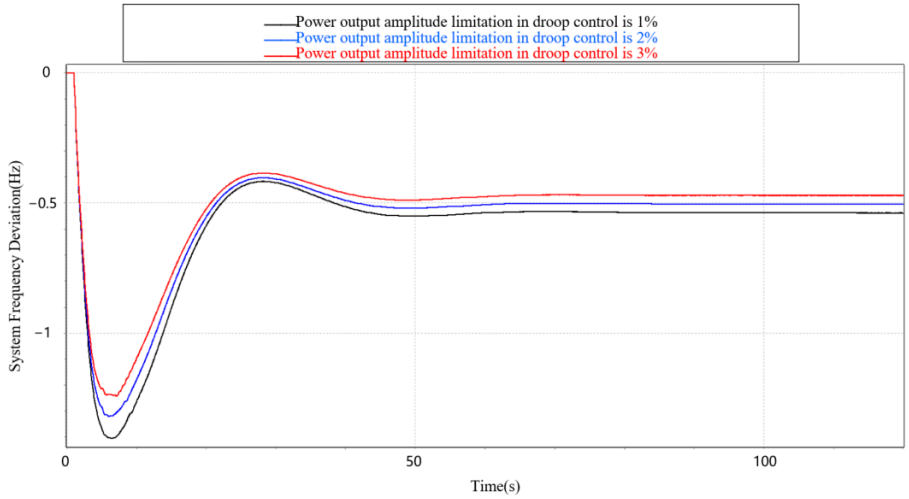


Figure 5. The influence of power output amplitude limitation in droop control on frequency stability.

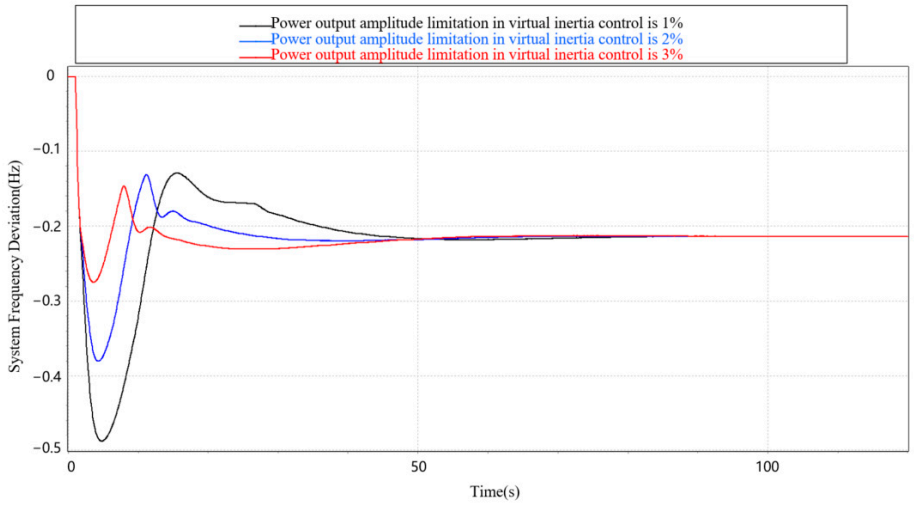


Figure 6. The influence of power output amplitude limitation in virtual inertia control on frequency stability.

It can be observed that, within the tested parameter range, the frequency stability of the system tends to improve with the increase in the virtual inertia coefficient, droop coefficient, virtual inertia control power limit, and droop control power limit. This observation is consistent with the trends predicted by the frequency response model analysis presented in the previous section. Specifically, within the investigated range, increasing the droop coefficient leads to a noticeable reduction in the steady-state frequency deviation following a disturbance. This can be explained by the fact that the droop coefficient reflects the amount of active power support that can be provided per unit of frequency deviation. A larger droop coefficient enhances the equivalent steady-state frequency regulation capability of the system. According to the static frequency–power balance relationship, this stronger regulation capability contributes directly to a smaller steady-state frequency deviation under the same active power imbalance. By contrast, virtual inertia control mainly affects the transient frequency response, particularly the maximum frequency deviation and the initial rate of change in frequency (RoCoF). Within the tested parameter range, increasing the virtual inertia coefficient and the virtual inertia control power limit enables the converter-interfaced source to release more active power during the initial stage of frequency variation, thereby slowing down frequency decline more effectively and improving transient frequency support. In general, its influence on the final steady-state

frequency deviation remains limited, since virtual inertia emulates inertial power exchange primarily during dynamic transients rather than by altering the long-term steady-state power balance. Nevertheless, further increases in these gain-related parameters, or excessively strong saturation/power-limit settings, do not necessarily continue to improve frequency stability. On the contrary, under certain conditions, especially in weak-grid scenarios, overly large gain coefficients may introduce adverse dynamic effects, such as increased overshoot, oscillatory responses, interaction with measurement filtering and RoCoF estimation, and even closed-loop instability.

3. Control Parameter Optimization Framework for Enhancing Frequency-Stable Support Capability

Based on the analysis in the previous section, key control parameters, such as the virtual inertia coefficient and the droop coefficient, have significant impacts on system frequency stability. To effectively enhance the frequency support capability of power systems, it is therefore necessary to optimize these control parameters. However, traditional parameter optimization methods based on time-domain simulation are computationally expensive, making it difficult to quickly assess the impact of parameters on frequency stability in complex operating scenarios. Therefore, this chapter first constructs a quantitative frequency stability margin index to accurately characterize the system's ability to withstand frequency instability. To address the challenge of efficiently evaluating the stability margin, an improved ResNet neural network-based mapping method for power system frequency stability margin is introduced, aiming to rapidly and accurately establish the complex nonlinear relationship between frequency control parameters and the system stability margin. On this basis, the trained neural network model is integrated into a control parameter optimization framework, forming a complete closed loop of evaluation–optimization. By employing Bayesian optimization under predefined power deficit levels and renewable energy penetration scenarios, various candidate frequency control parameter sets for renewable energy sources are generated, and the optimal control parameters that maximize the frequency stability margin are determined.

3.1. Quantification of Frequency Stability Margin

The typical process of power system frequency response is shown in Figure 7. The maximum rate of change in frequency, maximum frequency deviation, and steady-state frequency deviation correspond to the frequency response characteristics during the initial inertial response phase, intermediate dynamic phase, and steady-state phase of frequency dynamics, respectively. To ensure the safe and stable operation of the power grid, it is necessary to guarantee that the system frequency meets operational requirements throughout all time periods of the dynamic process following a disturbance. In practical grid operation, the initial frequency dip must be kept within a controlled range to avoid premature activation of underfrequency load shedding. It was selected in this study as an engineering security threshold with reference to GB/T 40596-2021 [27], which states that the frequency trigger value should preferably not exceed 49.25 Hz. Meanwhile, the steady-state limit of 0.2 Hz is consistent with the commonly used normal operating band of 49.8–50.2 Hz in 50 Hz systems, as reflected in GB/T15945-2008 [28] operation criteria.

Therefore, the frequency stability margin is set as follows:

$$c = \frac{\left|\overline{\Delta f_{\max}}\right| - |\Delta f_{\max}|}{\left|\overline{\Delta f_{\max}}\right|} \tag{5}$$

$$d = \frac{\left|\overline{\Delta f_s}\right| - |\Delta f_s|}{\left|\overline{\Delta f_s}\right|} \tag{6}$$

In the equation, $\Delta f_{\max}$ represents the actual maximum frequency deviation of the system. $\overline{\Delta f_{\max}}$ denotes the maximum permissible frequency deviation limit of the system, according to GB/T 40596-2021 [27], this value is 0.75 Hz. Δf_s represents the actual steady-state frequency deviation of the system; $\overline{\Delta f_s}$ denotes the permissible steady-state frequency deviation limit of the system, according to GB/T15945-2008, this value is 0.2 Hz. When the calculated margin is negative, it means that the corresponding frequency limit has been violated, indicating that the system does not satisfy the stability requirement under that condition.

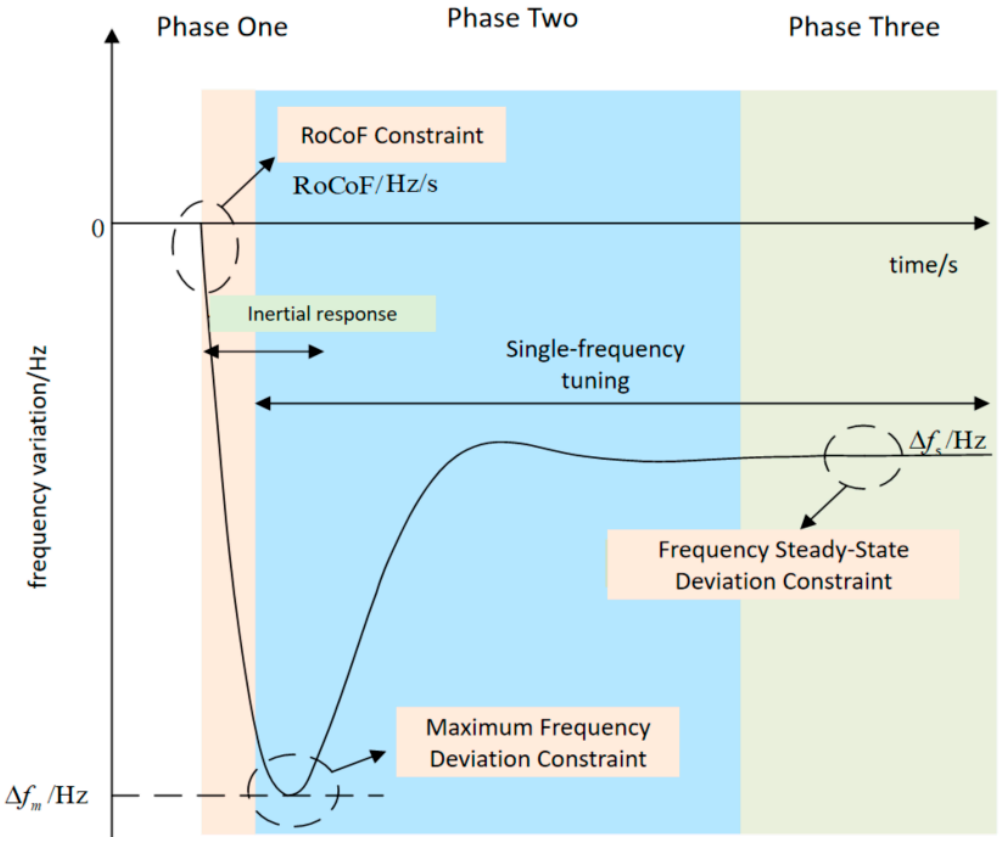


Figure 7. Full frequency response process.

3.2. Improved ResNet-Based Model for Power System Frequency Stability Margin Evaluation

This section employs an improved ResNet convolutional neural network approach to evaluate frequency stability margin. Given ResNet's advantages in addressing gradient explosion and vanishing gradient issues, and considering the highly nonlinear and coupled mapping relationship between features such as system operating conditions, control parameters and frequency stability margin, this network can better learn complex relationships by stacking deeper structures while maintaining training stability. To address offline analysis requirements for system frequency stability, this paper integrates the complementary strengths of ResNet and 1D-CNN to construct an enhanced ResNet composite network model with hybrid feature extraction capabilities. This model analyzes the complex, high-dimensional nonlinear relationship between input control/operating parameters and output frequency stability metrics, enabling regression prediction of frequency deviation. As shown in Figure 8, the core architecture of the improved ResNet consists of an input layer, ResNet layers, pooling layers, and an output layer.

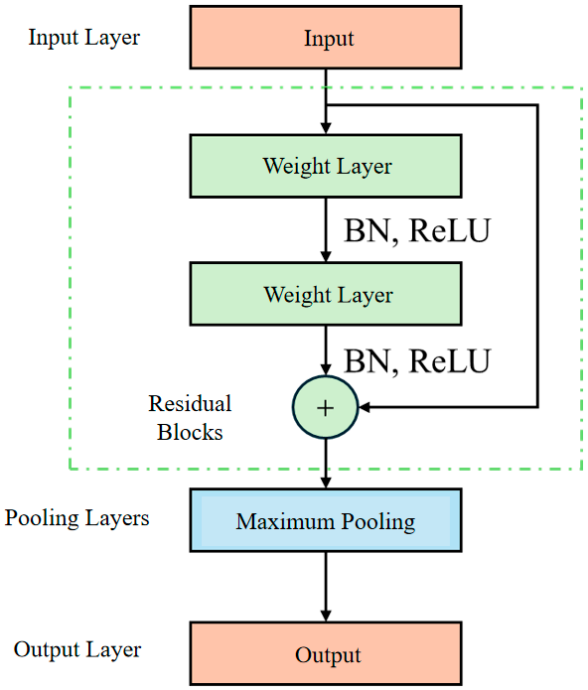


Figure 8. Architecture of the improved ResNet.

(1) Input Layer

Specifically, the input layer receives a feature vector composed of predefined system states and control parameters, including system power deficit, fault type, new energy penetration rate, droop coefficient, droop control power output upper limit amplitude, virtual inertia coefficient, and virtual inertia control power output upper limit amplitude.

(2) ResNet Layer

When network depth increases significantly, CNNs may experience phenomena such as gradient vanishing and feature degradation, limiting their ability to represent high-dimensional nonlinear systems. ResNet reconstructs traditional feedforward structures into a residual function learning paradigm by introducing cross-layer connections to build identity mappings, enabling the stable training of deep networks through modular stacking of residual blocks. Typical deep residual architectures employ a cascading arrangement of multilevel residual units, each containing a composite path comprising learnable residual components and identity mapping components.

ResNet possesses dual advantages in gradient flow optimization and model regularization, enabling it to effectively capture high-dimensional complex features. However, it cannot be directly applied to one-dimensional sequences. Therefore, this paper reconstructs the classic ResNet block by integrating it with 1D-CNN. The reconstructed ResNet block topology is illustrated in Figure 9.

A rectified linear unit (ReLU) is employed as the activation function, while a batch normalization (BN) layer is used to standardize the input feature distribution and suppress internal covariate shifts. The output of the ResNet block can be expressed as:

$$\boldsymbol{X}_o(N_o, L_o) = F(\boldsymbol{X}_u(N_u, L_u)) + \boldsymbol{X}_u(N_u, L_u) \tag{7}$$

In the equation, $\boldsymbol{X}_u(N_u, L_u)$ represents the one-dimensional input information, with N_u, L_u denoting the number and length of input channels, respectively; $F(\cdot)$ is the one-dimensional convolution operation function; $\boldsymbol{X}_o(N_o, L_o)$ represents the one-dimensional output information, with N_o, L_o denoting the number and length of output channels, respectively.

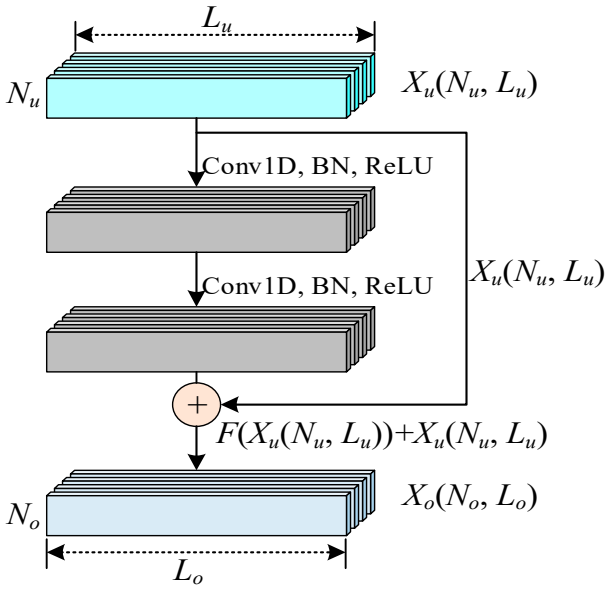


Figure 9. Improved 1D-ResNet Block.

At the network architecture level, ResNet layers employ a deep stacking strategy, with the number of layers dynamically optimized through cross-validation. This approach adapts to frequency deviation prediction tasks across power systems of varying scales. The output of the ResNet layers is as follows:

$$\boldsymbol{X}_{out} = \text{ResNet}(\boldsymbol{X}_u) \tag{8}$$

In the equation, ResNet(·) denotes the process of computing multiple ResNet blocks via Equation (7).

(3) Pooling Layer

The core function of the pooling layer lies in compressing the dimensionality of the feature space extracted by the convolutional kernel. In engineering practice, two typical operation operators—max pooling and average pooling—are widely adopted. The former enhances feature robustness by extracting local extreme values, while the latter reduces noise sensitivity through smoothing processing. The proposed model ensures generalization capability through max pooling, whose mathematical representation can be defined as:

$$\boldsymbol{P} = \max(\boldsymbol{X}_{out}) + \boldsymbol{b} \tag{9}$$

(4) Output Layer

During the output mapping phase, high-dimensional feature vectors are converted into predicted system frequency deviation values. To suppress model overfitting, randomly inactive units are embedded. By randomly blocking parameter update paths for some neurons during forward propagation, the network is forced to develop redundant feature representation mechanisms, thereby enhancing the model's generalization performance. Furthermore, to minimize the loss function of the neural network model, backpropagation of errors is commonly used for parameter updates. Optimal parameters are obtained through iterative training. Key algorithms and their variants include: Stochastic Gradient Descent (SGD), Stochastic Gradient Descent with Momentum (SGDM), Adaptive Gradient Algorithm (Adagrad), Root Mean Square Propagation (RMSProp), and Adam (Adaptive Moment Estimation). Among these, the Adam algorithm proposed as an extension of SGD

is currently the most widely used and effective. It achieves adaptability by estimating first- and second-order momentum of gradients.

From the sample set, 80% of the samples were selected as the training dataset, with the remaining 20% serving as the test dataset. Regression predictions for the system's maximum frequency deviation and steady-state frequency deviation were performed using the improved ResNet network. The proposed ResNet-based predictor consists of three residual blocks, and each block contains two convolutional layers. The numbers of channels in the three blocks are set to 32, 64, and 128, respectively. For all convolutional layers, the kernel size is 3 and the stride is 1. During training, the batch size is set to 32, and the network parameters are optimized using the AdamW optimizer with an initial learning rate of 1×10^{-3}. A ReduceLROnPlateau learning-rate schedule is adopted to adaptively decrease the learning rate when the validation performance stops improving. The maximum number of training epochs is 200, and an early stopping strategy with patience = 20 is employed to avoid overfitting. In addition, from the 6480 training samples, 15% are further split as a validation set for hyperparameter tuning and early stopping monitoring.

Model performance metrics adopted in this paper include Mean Square Error (MSE), Root Mean Square Error (RMSE), Mean Absolute Error (MAE), and Mean Absolute Percentage Error (MAPE), calculated as follows:

$$\mathrm{MSE} = \frac{1}{n}\sum_{j=1}^{n}\left(y'_j - y_j\right)^2 \tag{10}$$

$$\mathrm{RMSE} = \sqrt{\frac{1}{n}\sum_{j=1}^{n}\left(y'_j - y_j\right)^2} \tag{11}$$

$$\mathrm{MAE} = \frac{1}{n}\sum_{j=1}^{n}\left|y'_j - y_j\right| \tag{12}$$

$$\mathrm{MAPE} = \frac{1}{n}\sum_{j=1}^{n}\frac{\left|y'_j - y_j\right|}{\left|y'_j\right|} \tag{13}$$

In the formula, n denotes the total number of samples in the test set; the subscript j represents the jth test sample; y' indicates the predicted value; and y denotes the actual value. Each metric value is positively correlated with the overall error level of frequency deviation prediction. A lower metric value indicates lower prediction error, signifying better model performance.

3.3. Bayesian Optimization for Optimal Parameter Searching

Bayesian Optimization (BO) is a global optimization method for black-box functions, particularly suited for optimization problems where objective function evaluation is costly, non-differentiable, or noisy. Its fundamental principle involves constructing a probabilistic surrogate model of the objective function using acquired sample data in each iteration. By balancing exploration and exploitation through an acquisition function, it rapidly converges to the global optimum with fewer function evaluations. Since the frequency stability margin assessment in this paper can be rapidly provided by data-driven models, and the optimization variables (droop coefficient, virtual inertia coefficient, and their power limits) are all continuous parameters, Bayesian optimization enables efficient searches for the control parameter combination that maximizes the frequency stability margin within a finite number of iterations.

Specifically, let the vector of control parameters to be optimized be as follows:

$$\mathbf{x} = [x_1, x_2, \ldots, x_D]^{\mathrm{T}}, \mathbf{x} \in \Omega \subset \mathbb{R}^D \tag{14}$$

Here, D denotes the parameter dimension, and Ω denotes the feasible region of parameters. Let the objective function be the frequency stability margin M(x) (output by the improved ResNet mapping model in this paper). Then, the objective of Bayesian optimization is as follows:

$$\mathbf{x}^* = \underset{\mathbf{x}\in\Omega}{\operatorname{argmax}} M(\mathbf{x}) \tag{15}$$

Employ Gaussian Processes (GP) as a surrogate model. Treat the objective function as a stochastic process:

$$M(\mathbf{x}) \sim \mathcal{GP}\left(\mu(\mathbf{x}), k(\mathbf{x}, \mathbf{x}')\right) \tag{16}$$

In the equation, $\mu(\mathbf{x})$ denotes the mean function, and $k(\mathbf{x}, \mathbf{x}')$ denotes the covariance kernel function. Suppose a dataset has been sampled.

$$\mathcal{D}_t = \{(\mathbf{x}_i, y_i)\}_{i=1}^{t}, y_i = M(\mathbf{x}_i) + \varepsilon_i \tag{17}$$

Here, ε_i denotes the observation noise. According to GP posterior inference, for any candidate point x, the posterior distribution of the objective function can be expressed as:

$$M(\mathbf{x}) \mid \mathcal{D}_t \sim \mathcal{N}\left(\mu_t(\mathbf{x}), \sigma_t^2(\mathbf{x})\right) \tag{18}$$

Here, $\mu_t(\mathbf{x})$ and $\sigma_t(\mathbf{x})$ represent the predicted mean and uncertainty at iteration t, respectively.

To determine the next evaluation point, Bayesian optimization selects new candidate parameters by maximizing the acquisition function. This paper adopts the UCB framework, defined as:

$$\alpha_{\mathrm{UCB}}(\mathbf{x}) = \mu_t(\mathbf{x}) + \kappa\sigma_t(\mathbf{x}) \tag{19}$$

In the formula, $\boldsymbol{\kappa}$ is the coefficient balancing exploration and exploitation. A larger $\boldsymbol{\kappa}$ favors exploring regions of high uncertainty, while a smaller $\boldsymbol{\kappa}$ favors exploiting regions near the current optimal solution. The sampling point for iteration t+1 is then determined by the following equation:

$$\mathbf{x}_{t+1} = \underset{\mathbf{x}\in\Omega}{\operatorname{argmax}} \alpha_{\mathrm{UCB}}(\mathbf{x}) \tag{20}$$

The iterative process of Bayesian optimization can be summarized as follows: First, generate an initial sample set within the feasible domain using random or Latin hypercube sampling. Subsequently, in the *t*th iteration, train/update the GP surrogate model based on Dt, compute the objective function, and select new candidate solutions using the above equation. The frequency stability margin mapping model is invoked to obtain $y_{t+1} = M(\mathbf{x}_{t+1})$ and update the dataset.

$$\mathcal{D}_{t+1} = \mathcal{D}_t \cup \{(\mathbf{x}_{t+1}, y_{t+1})\} \tag{21}$$

Stop iteration when the maximum iteration count is reached or the convergence condition is satisfied, and output the optimal control parameters:

$$\mathbf{x}^* = \arg \max_{(\mathbf{x}_i, y_i)\in\mathcal{D}_{n_{\max}}} y_i \tag{22}$$

In this study, the Bayesian optimization procedure is implemented over four continuous control parameters. The optimization objective is formulated as a weighted sum of the

two predicted frequency stability margins, so that both transient and steady-state frequency performance can be considered simultaneously within a unified scalar objective function.

For the surrogate model, a Gaussian process with a Matérn 5/2 kernel equipped with automatic relevance determination (ARD) is adopted. This kernel provides sufficient flexibility for representing the nonlinear relationship between the control parameters and the predicted stability margins, while ARD allows the model to adaptively characterize the relative sensitivity of different optimization variables through individual length-scale parameters.

The acquisition function is selected as the Upper Confidence Bound (UCB), with the exploration parameter set to $\kappa = 2.0$. This choice provides a practical balance between exploration of uncertain regions and exploitation of regions with promising predicted objective values, thereby improving the search efficiency of the BO process.

To initialize the optimization, 12 initial sample points are generated using Latin hypercube sampling (LHS), which ensures relatively uniform coverage of the decision space. Based on these initial samples, the BO algorithm is then iterated for 400 optimization steps to progressively identify the control parameter combination with superior frequency stability performance.

3.4. Formulation of the Frequency Control Parameter Optimization Model

Larger virtual inertia and droop coefficients typically imply stronger support for additional frequencies, but also correspond to higher control input, greater power regulation requirements, and increased equipment stress. This paper focuses not only on improving frequency stability margin during optimization but also tends to select smaller parameter values while ensuring frequency safety and maximizing stability margin as much as possible. This approach prevents the optimization results from tending toward the upper bounds of the parameters without constraints, and ensures that the resulting control parameters are more economical, feasible, and suitable for engineering applications. Therefore, the optimization model whose objective is a weighted single-objective function is constructed as follows:

$$\begin{aligned} &\max \omega_1 \frac{\left|\overline{\Delta f_{\max}}\right| - |\Delta f_{\max}|}{\left|\overline{\Delta f_{\max}}\right|} + \omega_2 \frac{\left|\overline{\Delta f_s}\right| - |\Delta f_s|}{\left|\overline{\Delta f_s}\right|} - \omega_3 \frac{K_i}{K_i^{\max}} - \omega_4 \frac{K_d}{K_d^{\max}} \\ &s.t. \begin{cases} |\Delta f_{\max}| \le \left|\overline{\Delta f_{\max}}\right| \\ |\Delta f_s| \le \left|\overline{\Delta f_s}\right| \\ \Delta P_d^{\max} + \Delta P_i^{\max} \le \overline{\Delta P_{\max}} \\ \overline{\Delta P_{\min}} \le \Delta P_d^{\min} + \Delta P_i^{\min} \\ 0 \le K_i \le K_i^{\max} \\ 0 \le K_d \le K_d^{\max} \end{cases} \end{aligned} \tag{23}$$

In the equation, $\Delta f_{\max}$ represents the maximum frequency deviation after a fault occurs; $\overline{\Delta f_{\max}}$ denotes the maximum permissible frequency deviation to ensure frequency stability; Δf_s represents the steady-state frequency deviation after a fault occurs; $\overline{\Delta f_s}$ denotes the maximum permissible steady-state frequency deviation to ensure frequency stability; $\Delta P_i^{\max}$ and $\Delta P_d^{\max}$ represent the upper limit amplitudes of power output for virtual inertia control and frequency droop control. $K_i^{\max}$ is the maximum virtual inertia coefficient; $K_d^{\max}$ is the maximum droop coefficient; $\overline{P_{\max}}$ represents the maximum permissible upper power output limit for the additional frequency control of the new energy generation system; $\overline{P_{\min}}$ represents the maximum permissible lower power output limit for the additional frequency control of the new energy generation system; ω_1, ω_2, ω_3, ω_4 are weighting factors.

The frequency control parameter optimization strategy framework is shown in Figure 10. The proposed framework is systematically divided into two interconnected stages: the data

preparation and model training stage (left) and the parameter optimization stage (right). The complete workflow is detailed as follows.

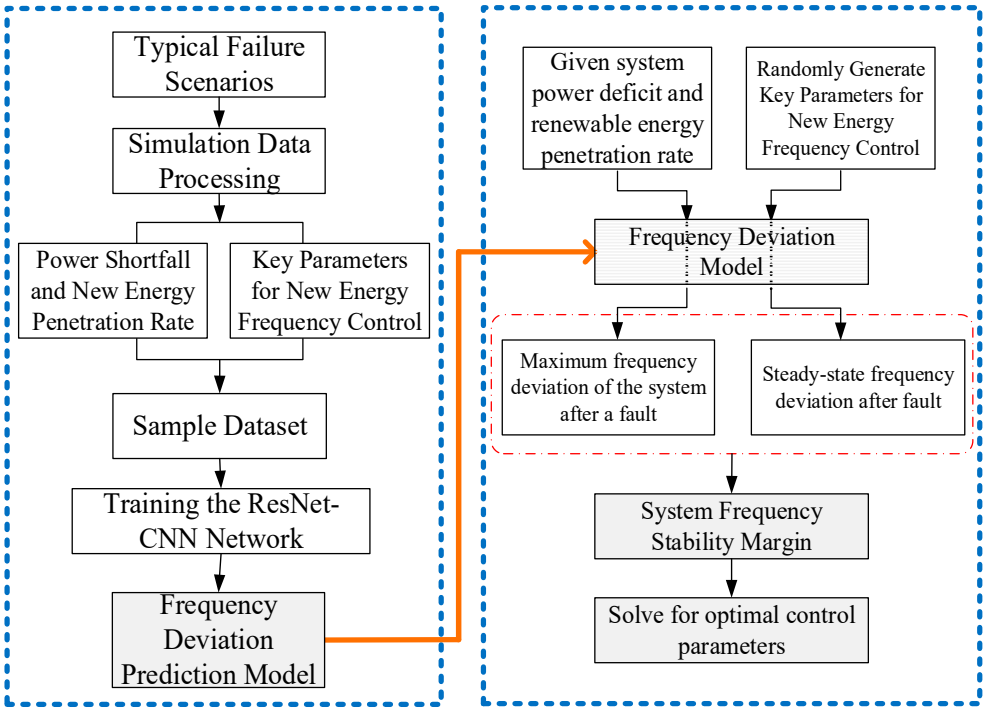


Figure 10. Frequency Control Parameter Optimization Strategy.

Stage 1: Data preparation and frequency deviation prediction model training

This stage aims to develop a fast and accurate surrogate model that maps control parameters to frequency response metrics. First, by considering factors such as system power deficit, renewable energy penetration rate, and the key parameters for renewable energy frequency control, a set of typical large-disturbance fault scenarios is established. For each scenario, time-domain simulations are conducted under various combinations of system power deficit levels and renewable energy penetration rates. From the simulation results, critical output metrics, namely, the maximum frequency deviation and the steady-state frequency deviation, are extracted. This collection of input–output pairs forms a comprehensive sample dataset. Subsequently, this dataset is used to train the improved ResNet network. Through iterative training, where prediction performance is monitored and network hyperparameters are adjusted, a frequency deviation prediction model is ultimately developed. This model serves as a computationally efficient digital twin for frequency response evaluation.

Stage 2: Parameter optimization based on the prediction model

Based on the trained frequency deviation prediction model, Bayesian optimization is employed to iteratively generate candidate sets of renewable energy frequency control parameters under the given system power deficit and renewable energy penetration rate. Each candidate parameter set is evaluated by the prediction model, which outputs the corresponding frequency stability metrics. The optimization algorithm iteratively refines its search strategy based on these evaluations. This process continues until convergence, ultimately solving for the optimal control parameters that maximize the system's frequency stability margin.

4. Case Study

In the previous section, key frequency response indicators, including the maximum frequency deviation and steady-state frequency deviation, were extracted from time-domain

simulation results under different combinations of power deficit levels and renewable energy penetration ratios to construct an input–output dataset. Based on this dataset, an improved ResNet network was trained to develop a fast prediction model for evaluating the frequency stability margin. Subsequently, Bayesian optimization was integrated with the trained predictor to iteratively generate candidate control parameter sets and adaptively update the search strategy according to the evaluation results until the optimal control parameters were obtained. On this basis, a complete frequency control parameter optimization framework was established. To further validate the prediction accuracy of the proposed optimization model and its effectiveness in improving frequency stability, case studies were conducted on the CSEE-FS low-frequency test system, which already incorporates dynamic factors such as load damping and turbine delays. Therefore, this study focuses on the influence of virtual inertia and droop-related parameters under the existing system configuration. Moreover, the proposed framework is inherently scalable to larger power systems, since the same methodology can be extended once new datasets are generated from larger simulation systems and used to retrain the predictor.

4.1. Accuracy Verification of the Improved ResNet-Based Power System Frequency Stability Margin Prediction

This paper employs an improved ResNet-based convolutional neural network architecture. This architecture comprises an input layer for feature input and representation, the improved ResNet feature extraction module, which achieves hierarchical feature extraction by stacking multiple residual blocks, and a fully connected output layer for regression computation. Benefiting from the residual connection mechanism, this network architecture effectively mitigates gradient explosion and network degradation issues that may arise during deep network training, thereby ensuring the stability and efficiency of deep feature learning. After training the network using the constructed sample dataset, the proposed improved ResNet model accurately learns the complex high-dimensional nonlinear mapping relationship between key control parameters, operational parameters, and the system's frequency stability margin, enabling efficient evaluation of the power system's frequency stability margin. The specific parameter settings for the sample dataset are shown in the table below. A total of 8100 simulation samples were generated using a grid sampling strategy. For each sample, time domain simulation was performed with a timestep of 0.02 s and a simulation duration of 150 s. Three disturbance types were considered, namely, cutting machines, cutting new energy, and sudden load increase, as listed in Table 1. In the neural network input, the disturbance type was encoded as 1, 2, and 3, respectively.

Table 1. System Frequency Stability Sample Set Parameter Settings.

Parameters	Selection Range
New Energy Penetration Rate	[30%, 60%]
Power deficit	[200 MW, 600 MW]
Fault Type	Cutting machines, cutting new energy, sudden load increase
Virtual Inertia Coefficient	[10, 30]
Virtual Inertia Control Power Output Upper Limit Amplitude	[0%, 15%]
Droop Coefficient	[10, 50]
Droop Control Power Output Upper Limit Amplitude	[0%, 15%]

To validate the superiority of the proposed network model over traditional neural network models, this paper introduces backpropagation (BP), decision transformers (DT), and convolutional neural networks (CNN) for comparison. The prediction performance

of the improved ResNet network for maximum frequency deviation and steady-state frequency deviation is shown in Tables 2 and 3 and Figures 11 and 12. It can be seen that the proposed frequency stability margin prediction method can rapidly and effectively analyze system frequency stability, and its predictive performance is superior to that of classical network models.



Figure 11. Predicted Transient Frequency Stability Margin Results.

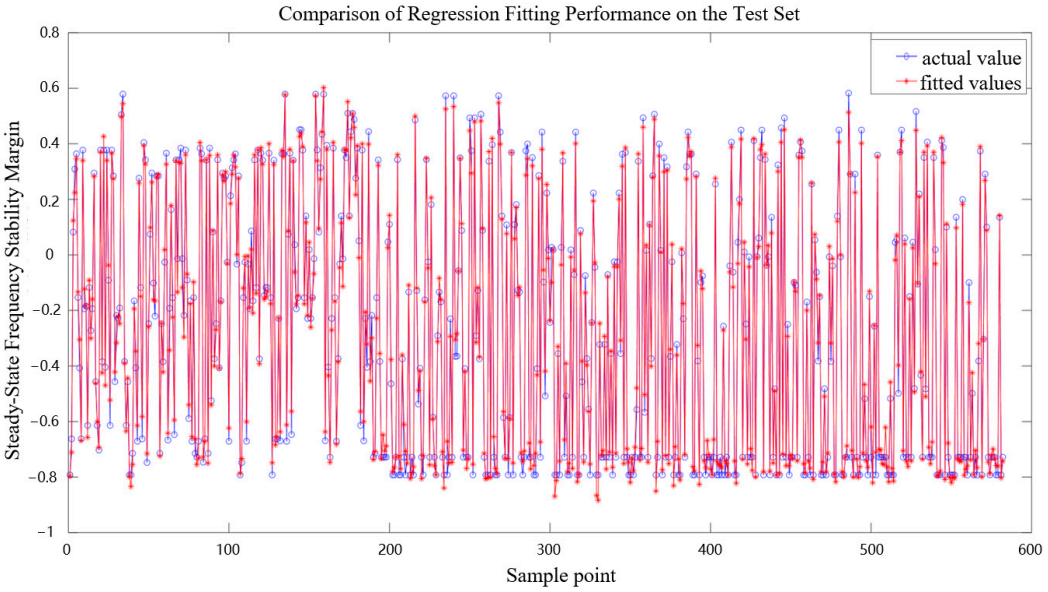


Figure 12. Steady-State Frequency Stability Margin Prediction Results.

Table 2. Maximum Frequency Deviation Test Set Prediction Performance.

Prediction Model	MSE/Hz	RMSE/Hz	MAE/Hz	MAPE/%
BP	0.0542	0.4674	0.2152	5.56
DT	0.0313	0.2739	0.1946	5.16
CNN	0.0204	0.1903	0.0876	2.87
Improved ResNet	0.0101	0.1005	0.0771	2.74

Table 3. Steady-State Frequency Deviation Test Set Prediction Performance.

Prediction Model	MSE/Hz	RMSE/Hz	MAE/Hz	MAPE/%
BP	0.0029	0.0713	0.0445	4.97
DT	0.0023	0.0637	0.0378	3.81
CNN	0.0011	0.0323	0.0228	2.94
Improved ResNet	0.0008	0.0275	0.0217	2.80

4.2. Validation of Parameter Optimization Model Effectiveness

For different renewable energy penetration levels, with a fixed frequency–modulation deadband of 0.03 Hz, different control parameter combinations were randomly generated using Bayesian algorithms. Based on the frequency margin prediction model, the transient and steady-state frequency stability margins for each parameter combination were forecasted and optimized. The final solution yielded optimal control parameters that maximize system frequency stability margins under varying renewable penetration levels, considering different fault types and power deficits, as shown in Table 4.

Table 4. Optimized Frequency Control Parameters Under Different Renewable Penetration.

Renewable Penetration	Droop Coefficient	Droop Control Power Output Upper Limit Amplitude (p.u.)	Virtual Inertia Coefficient	Virtual Inertia Control Power Output Upper Limit Amplitude
40%	45.54	0.064	30	0.036
50%	48.21	0.077	28.38	0.023
60%	49.68	0.085	26.14	0.015

To validate the effectiveness of parameter optimization in enhancing system frequency stability, we compared the performance of a system without virtual inertia control. This was performed under a scenario where renewable energy accounts for 65% of installed capacity, which exceeds the sample penetration range, thereby verifying robustness against random uncertainties. We compared the frequency performance of a system with frequency control parameters set to the optimized values against that of a system with a droop coefficient of 50 and a droop control power output upper limit amplitude of 0.1 p.u. prior to optimization. The frequency control performance is illustrated in Figure 13, while the enhancement in frequency stability margin is summarized in Table 5. In addition, to further demonstrate the effectiveness of the proposed optimization framework, the convergence curves of Bayesian optimization, particle swarm optimization (PSO), and the genetic algorithm (GA) are shown in Figure 14. The results indicate that BO achieves better optimization results.

As shown in the chart above, after optimizing the control parameters, the system's frequency stability improves.

Table 5. Comparison of Stability Margin Before and After Frequency Control Parameter Optimization.

	Transient Frequency Stability Margin	Steady-State Frequency Stability Margin	$RoCoF_{max}$	f_{nadir}	Settling Time
Original Scene	0.178	−0.342	−0.032	−0.591	108.7
Parameter Control Optimization Scene	0.501	0.084	−0.025	−0.343	59.6

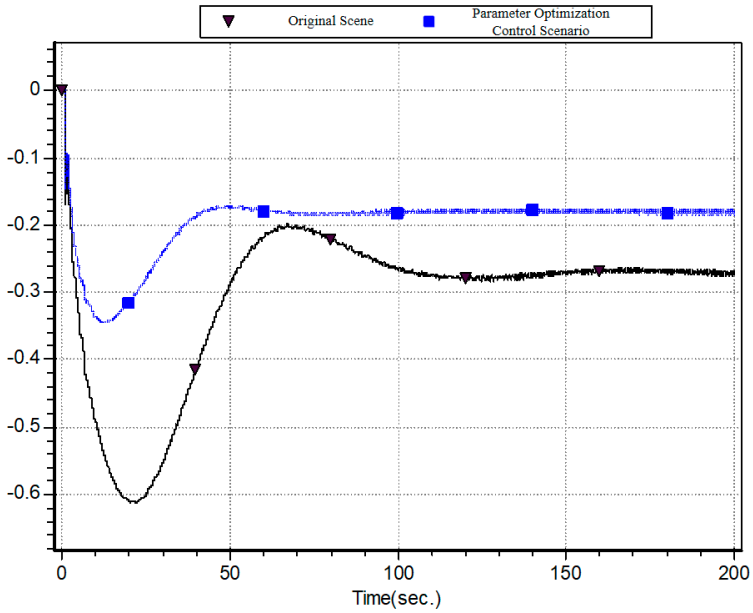


Figure 13. The Impact of Frequency Control Parameter Optimization Under a 250 MW Sudden System Load Increase.

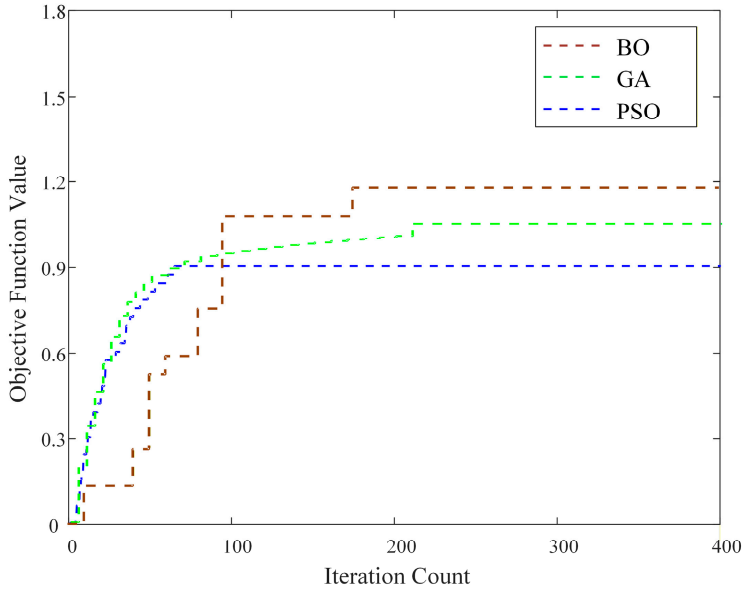


Figure 14. Comparison of Convergence Behavior Among Bayesian Optimization, Particle Swarm Optimization, and Genetic Algorithm.

5. Conclusions

This paper proposed a frequency stability assessment and parameter optimization framework for high-renewable power systems by integrating a second-order frequency response model, a data-driven frequency stability margin predictor, and a Bayesian optimization strategy. Specifically, frequency stability margins were constructed from the perspectives of transient and steady-state frequency performance, and an improved ResNet-based regression model was developed to establish the nonlinear mapping between system operating conditions, control parameters, and stability margins. On this basis, Bayesian optimization was employed to search for the virtual inertia and droop parameter combination that yields improved frequency stability performance. The overall framework provides a computationally efficient approach for fast frequency stability evaluation and coordinated parameter tuning under different disturbance scenarios. The results demonstrate that the

proposed method can effectively characterize the frequency stability of the system and provide an accurate quantitative prediction of frequency stability margins under varying renewable penetration levels, power imbalance conditions, and disturbance types. At the same time, the optimization results show that appropriate coordination of virtual inertia and droop parameters can effectively improve the system frequency stability margin. Specifically, under a specific coefficient selection, the transient frequency stability margin increased by 32.3%, and the steady-state frequency stability margin increased by 42.6%. Therefore, the proposed method is not only able to predict system frequency stability rapidly, but also capable of providing a feasible parameter-tuning basis for renewable-rich power systems, thereby offering potential support for online stability assessment and adaptive control parameter design.

Nevertheless, several limitations should be acknowledged. The SFR model is based on simplifying assumptions, including small-disturbance linearization, constant system parameters, and dominant low-order dynamics, which may limit its ability to capture nonlinear, time-varying, and higher-order characteristics of practical power systems. Moreover, as the proposed approach is data-driven, its generalization ability depends on the quality, coverage, and representativeness of the simulation-labeled dataset. Future work may further compare the proposed framework with other surrogate models and optimization methods such as deep multilayer perceptrons, Gaussian process variants, and genetic algorithms to better clarify its advantages and limitations. In addition, it can be extended to practical applications such as online frequency stability screening, rapid emergency support assessment, and adaptive parameter tuning for converter-based renewable resources in low-inertia power systems.

In summary, this work provides a combined modeling, prediction, and optimization framework for frequency stability analysis in renewable-dominated power systems. The study verifies the feasibility of using a data-driven predictor to replace repeated time-domain simulations for rapid stability-margin evaluation and parameter optimization. Although further improvement is still needed in model generalization, uncertainty handling, and large-scale validation, the proposed method offers a useful basis for future research on intelligent frequency stability assessment and control parameter coordination in modern power systems.

Author Contributions: Conceptualization, Z.X., Z.Z. and G.L.; Methodology, L.C., F.Y. and J.R.; Software, L.C. and F.Y.; Validation, L.C., Z.X., J.R. and G.L.; Formal analysis, F.Y. and Z.Z.; Investigation, L.C., F.Y. and Z.Z.; Resources, L.C., Z.X. and J.R.; Data curation, L.C. and Z.X.; Writing—original draft, L.C. and F.Y.; Writing—review & editing, L.C., J.R. and G.L.; Supervision, Z.Z. and G.L. All authors have read and agreed to the published version of the manuscript.

Funding: This research was funded by the Science and Technology Project of Northwest Branch of State Grid Corporation of China (Research on the evolutionary trends of typical annual stability characteristics in the new power system of northwest China, SGNW0000DKJS2500199).

Data Availability Statement: The original contributions presented in this study are included in the article. Further inquiries can be directed to the corresponding author.

Conflicts of Interest: Authors Zhou Xing and Jing Ren were employed by the company Northwest Branch of State Grid Corporation of China. The remaining authors declare that the research was conducted in the absence of any commercial or financial relationships that could be construed as a potential conflict of interest. The authors declare that this study received funding from Science and Technology Project of Northwest Branch of State Grid Corporation of China. The funder had the following involvement with the study: Zhou Xing and Ren Jing are employees of this organization and contributed to the preparation of this paper, including the conception, methodological design, data validation, resource provision, data curation, and review and editing.

References

1. Qin, B.Y.; Hong, S.D.; Wang, H.Z. Non-isothermal Dynamic Model and Collaborative Optimization for Multi-energy System Considering Pipeline Energy Storage. *J. Energy Storage* **2026**, *141*, 119083. [CrossRef]
2. Qin, B.Y.; Wang, H.Z.; Li, F.; Liu, D.; Liao, Y.; Li, H.Y. Towards Zero Carbon Hydrogen: Co-Production of Photovoltaic Electrolysis and Natural Gas Reforming with CCS. *Int. J. Hydrogen Energy* **2024**, *78*, 604–609. [CrossRef]
3. Morren, J.; De Haan, S.W.H.; Kling, W.L.; Ferreira, J.A. Wind turbines emulating inertia and supporting primary frequency control. *IEEE Trans. Power Syst.* **2006**, *21*, 433–434. [CrossRef]
4. Qin, B.Y.; Wang, H.Z.; Liao, Y.; Li, H.; Ding, T.; Wang, Z.D.; Li, F.; Liu, D. Challenges and opportunities for long-distance renewable energy transmission in China. *Technol. Assess.* **2024**, *69*, 103925. [CrossRef]
5. Wang, H.Z.; Qin, B.Y.; Hong, S.D.; Xu, X.; Su, Y.W.; Lu, T.X.; Ding, T. Enhanced GAN Based Joint Wind-Solar-Load Scenario Generation With Extreme Weather Labelling. *IEEE Trans. Smart Grid* **2025**, *16*, 4213–4224. [CrossRef]
6. Wang, H.Z.; Qin, B.Y.; Su, Y.N. Coordinated Planning of Mobile Electric-hydrogen Energy Storage for Remote Power System Resilience Enhancement. *J. Energy Storage* **2026**, *147*, 120160. [CrossRef]
7. Wang, H.Z.; Qin, B.Y.; Hong, S.D.; Cai, Q.C.; Li, F.; Ding, T.; Li, H.Y. Optimal planning of hybrid hydrogen and battery energy storage for resilience enhancement using bi-layer decomposition algorithm. *J. Energy Storage* **2025**, *110*, 115367. [CrossRef]
8. Li, H.Y.; Qin, B.Y.; Wang, S.H.; Ding, T.; Liu, J.L.; Wang, H.Z. Aggregate power flexibility of multi-energy systems supported by dynamic networks. *Appl. Energy* **2025**, *377*, 124565. [CrossRef]
9. Zhang, H.X.; Li, C.G.; Liu, Y.T.; Huang, Z.L.; Zhuang, K.Q. Reviews on power system dynamic frequency analysis and its application. *Trans. China Electrotech. Soc.* **2010**, *25*, 169–176.
10. Qin, B.Y.; Liu, J.L.; Wang, H.Z.; Wang, Z.J.; Xiong, Z.M.; Wang, M.Y.; Qian, Q.H. Energy-efficient and reliable urban rail transit: A new framework incorporating underground energy storage systems. *iEnergy* **2025**, *4*, 86–97. [CrossRef]
11. Wang, H.Z.; Qin, B.Y.; Su, Y.W.; Li, F.; Hong, S.D.; Wang, Y.; Ding, T. Dynamic Carbon Market Driven Multi-Stage Scheduling Strategy for Hydrogen Integrated Energy Systems. *Renew. Energy*, 2026, *in press*. [CrossRef]
12. Qin, B.Y.; Li, H.Y.; Wang, Z.J.; Jiang, Y.; Lu, D.C.; Du, X.L.; Qian, Q.H. New framework of low-carbon city development of China: Underground space based integrated energy systems. *Undergr. Space* **2024**, *14*, 300–318. [CrossRef]
13. Wang, M.J.; Guo, J.B.; Ma, S.C.; Wang, T.; Zhang, X.; Luo, K.; Wang, G.Z. Review of transient frequency stability analysis and frequency regulation control methods for renewable power systems. *Proc. CSEE* **2023**, *43*, 1672–1694.
14. Yu, W.; Yang, H.H.; Jiao, W. Adaptive virtual inertial control strategy of optical storage and distribution network based on TOPSIS algorithm. *J. Shanghai Jiao Tong Univ.* **2022**, *56*, 1317–1324.
15. Cao, Y.; Wang, W.; Li, Y. A Virtual Synchronous Generator Control Strategy for VSC-MTDC System. *IEEE Trans. Energy Convers.* **2017**, *33*, 750–761. [CrossRef]
16. Yao, W.Z.; Yang, M.J.; Zhang, H.L.; Wu, J.; Wang, L.; Cao, J. VSG Control and Its Modified Algorithm for VSC-HVDC Inverter Participating Grid's Frequency Regulation. *Proc. CSEE* **2017**, *37*, 525–533.
17. Shen, Z.P.; Zhu, J.B.; Ge, L.J. Variable-inertia emulation control scheme for VSC-HVDC transmission systems. *IEEE Trans. Power Syst.* **2022**, *37*, 629–639. [CrossRef]
18. Zhang, G.F.; Yang, J.Y.; Sun, F.; Ge, Y.; Xing, Z. Primary frequency regulation strategy of DFIG based on virtual inertia and frequency droop control. *Trans. China Electrotech. Soc.* **2017**, *32*, 225–232.
19. Li, S.H.; Li, Z.P.; Zhang, H.; Shang, Y.K.; Jiang, Y.T.; Song, Y. Optimization of DFIG control parameters based on extended trajectory sensitivity of wind power integrated power systems. *Acta Energiae Solaris Sin.* **2021**, *42*, 369–376.
20. Li, S.; Tao, D.; Li, L. Suppression to angular oscillation among synchronous generators by optimizing parameters and set-points of synchronous condenser and high-voltage DC. *Int. Trans. Electr. Energy Syst.* **2022**, *2022*, 9161590. [CrossRef]
21. Sun, D.W.; Liu, H.; Li, Y.H. Effect Mechanism of Primary Frequency and Virtual Inertia Control of Inverter Power on Low Frequency Oscillation in Wind-thermal/Solar-thermal Bundled System. *Proc. CSEE* **2021**, *41*, 5947–5957.
22. Yan, C.; Yao, W.; Cui, Y.; Sun, K.; Wen, J.; Guo, R. Small Disturbance Stability Analysis of Wind-thermal Coupling System Considering Virtual Inertia and Droop Control. *Electr. Power Autom. Equip.* **2022**, *42*, 19–28.
23. Fu, Y.; Wang, Y.; Zhang, X.Y.; Luo, Y. Analysis and integrated control of inertia and primary frequency regulation for variable speed wind turbines. *Proc. CSEE* **2014**, *34*, 4706–4716.
24. Li, H.Y.; Ju, P.; Gan, C. Analytic analysis for dynamic system frequency in power systems under uncertain variability. *IEEE Trans. Power Syst.* **2018**, *34*, 982–993. [CrossRef]
25. Zhang, Z.; Qin, B.Y.; Ding, T.; Gao, X.; Zhang, Y.X. CBAM-CNN Based Transient Overvoltage Preventive Control Considering Piecewise Linear Control Sensitivity. *IEEE Trans. Power Syst.* **2025**, *40*, 3645–3656. [CrossRef]
26. Qin, B.Y.; Chen, P.; Zhang, Z.; Wang, H.; Ding, T. Coordinated preventive control strategy for transient overvoltage suppression in hybrid AC/DC sending-side systems. *Int. J. Electr. Power Energy Syst.* **2025**, *171*, 111017. [CrossRef]

27. *GB/T 40596-2021*; Technical Requirements for Power System Wide-Area Oscillation Monitoring. Standardization Administration of China: Beijing, China, 2021.
28. *GB/T 15945-2008*; Power System Frequency Technical Requirements. Standardization Administration of China: Beijing, China, 2008.

Disclaimer/Publisher's Note: The statements, opinions and data contained in all publications are solely those of the individual author(s) and contributor(s) and not of MDPI and/or the editor(s). MDPI and/or the editor(s) disclaim responsibility for any injury to people or property resulting from any ideas, methods, instructions or products referred to in the content.